

Article

Llonomers-New Generation of Ionomer: Understanding of Their Interaction and Structuration as a Function of the Tunability of Cation and Anion

Liutong Hou, Sébastien Livi, Jean-François Gérard and Jannick Duchet-Rumeau *

Université de Lyon, CNRS, Université Claude Bernard Lyon 1, INSA Lyon, Université Jean Monnet, UMR 5223, Ingénierie des Matériaux Polymères, CEDEX, F-69621 Villeurbanne, France

* Correspondence: jannick.rumeau@insa-lyon.fr

Abstract: In this work, by combining maleic anhydride-grafted polypropylene (PPgMA) and three different ionic liquids (ILs), i.e., tributyl (ethyl) phosphonium diethyl phosphate (denoted P⁺DEP), 1-ethyl-3-methylimidazolium diethyl phosphate (denoted EMIM DEP), and 1-ethyl-3-methylimidazolium acetate (denoted EMIM Ac), new ionic PP/IL polymer materials are generated and denoted as Llonomers. The structuration of ILs in Llonomers occurs from a nano/microphase separation process proved by TEM. NMR analyses reveal the existence of ionic–ionic and ionic–dipolar interactions between PPgMA and ILs within Llonomers. The rheological behavior of such IL/polymer combinations interpret the existence of interactions between maleic anhydride group and cation or anion composing the ionic liquid. These interactions can be tuned by the nature of cation (P⁺DEP vs. EMIM DEP) and anion (EMIM DEP vs. EMIM Ac) but also depend on the IL content. Thermal analyses demonstrate that IL could affect the crystallization process according to different pathways. Thanks to the maleic anhydride/IL interactions, an excellent compromise between stiffness and stretchability is obtained paving the way for processing new polyolefin-based materials.

Keywords: Llonomers; ionomers; maleic anhydride grafted polypropylene; ionic liquids; ion and dipole interactions



Citation: Hou, L.; Livi, S.; Gérard, J.-F.; Duchet-Rumeau, J.

Llonomers-New Generation of Ionomer: Understanding of Their Interaction and Structuration as a Function of the Tunability of Cation and Anion. *Polymers* **2023**, *15*, 370. <https://doi.org/10.3390/polym15020370>

Academic Editor: Johannes Carolus (John) Jansen

Received: 10 November 2022

Revised: 29 December 2022

Accepted: 31 December 2022

Published: 10 January 2023



Copyright: © 2023 by the authors. Licensee MDPI, Basel, Switzerland. This article is an open access article distributed under the terms and conditions of the Creative Commons Attribution (CC BY) license (<https://creativecommons.org/licenses/by/4.0/>).

1. Introduction

In the past decades, large attention has been poured into the study of ionomers. Ionomers are polymers containing up to 15 molar% of ionic groups that are frequently carboxylic, phosphoric, or sulfonic acid anions neutralized by metal salts, i.e., zinc, sodium or potassium cations [3,4]. These materials display a multi-scale structuration: the ion-pairs formed between acids anions and metal salts, usually assemble to form multiple states and participate in ionic clusters. Such ionic structuration leads to a restricted motion of polymer chains [3,4]. Consequently, a significant improvement of molten and solid-state properties are realized thanks to the physical crosslinking points generated via ionic interactions [5–11]. This effect is strongly related to the ionic multiplets generated as a segregated phase as for polyurethanes [12]. The rheological behavior (as for sulfonated polystyrene [10]) as well as the final crystalline state could be strongly affected by the existence of ion-pairs interactions. This effect is also demonstrated for the glass transition and melt elasticity of PLA-based ionomers [13,14]. According to the same approach, ionomers have been processed from different polymers such as polybutadiene-co acrylic acid or ethylene-methacrylic acid copolymers neutralized by zinc cations. Using maleic anhydride-grafted polypropylene (PPgMA) as precursor to design ionomers neutralized by zinc acetate leads to an increase of the molten strength due to the generation of branched chain structures [15,16]. Ionomer-like materials could be also used as efficient compatibilizers in non-miscible PP/PE blends [17,18]. For maleic anhydride-grafted polymers, zinc acetate

and sodium hydrogen carbonate are usually considered. In fact, carboxylic functions generated from the hydration of the anhydride are known to interact with the corresponding cations. The establishment of interactions between grafted polyolefin chains and salts can be successfully realized via twin-screw extrusion. Such modification is demonstrated to be efficient for improving the elongation at break and impact properties. On the other hand, owing to the advantages of Ionic Liquids (ILs) such as thermal stability, non-flammability, and low saturated vapour pressure, they have been used as surfactants [19], plasticizers [20], compatibilizers [21], and structuring agents [22]. For example, 1-butyl-3-methyl imidazolium chloride could act as plasticizer and compatibilizer of starch/zinc blends, leading to smaller zinc aggregates [23]. Trihexyltetradecylphosphonium bis(trifluoromethylsulfonyl) imide and trihexyltetradecylphosphonium bis 2,4,4-(trimethylpentyl) phosphinate could serve as compatibilizers for thermoplastic blends (PP/PA6) [21]. In this study, ILs located at PP/PA interface behave as interfacial agents, resulting in the depressed size of dispersed phase and a decrease of the PP/PA interfacial tension. In fact, ionic liquids are promising components according to their intrinsic features and their ionic characters [19,24–26] which could promote interactions with polar groups.

Thus, a new generation of polypropylene-based ionomer is proposed for the first time in this study. New types of ionomers designed from Ionic Liquids (ILs) and maleic anhydride-grafted polypropylene (denoted as Llonomers) have been considered. An ionic interaction continuum must be generated from the interactions COO^- from PPgMA with the cation and the anion pairs of ILs. The microstructure shown in Figure 1 describes the targeted assembling of ionic liquid pairs leading to a percolated ionic species network within the grafted polyolefin matrix. This novel approach offers the way to tune the final Llonomers behavior by using different types of ILs. In this work, a phosphonium-based ionic liquid (PhIL), i.e., tributyl (ethyl)phosphonium diethyl phosphate (P^+DEP , owning small steric hindrance favouring the interaction with polar groups of polymer matrix) and two imidazolium-based ionic liquids (ImILs), i.e., 1-ethyl-3-methylimidazolium diethyl phosphate (EMIM DEP) and 1-ethyl-3-methylimidazolium acetate (EMIM Ac), have been considered to investigate the role of cation, phosphonium vs. imidazolium and the role of anion, acetate vs. diethyl phosphate. This paper proposes to explore how (i) ILs generate ionic–ionic/dipole interactions with PPgMA, (ii) ionic–ionic/dipole interactions influence the PPgMA crystallization process and morphologies as well as consequently mechanical properties.

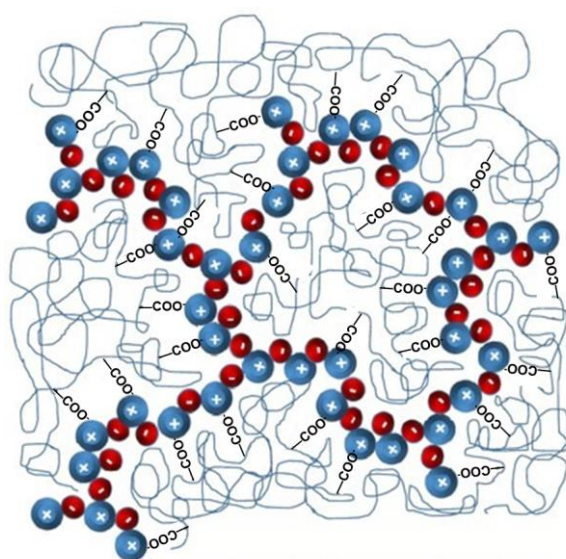
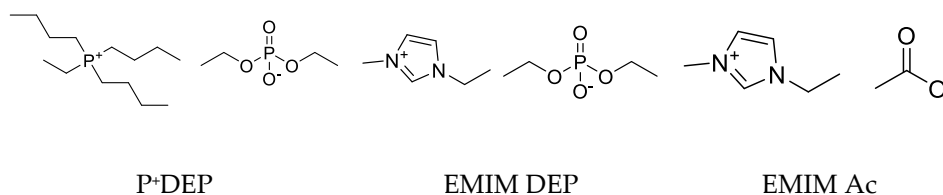


Figure 1. Targeted nano/microstructure of Llonomers.

2. Experimental Section

2.1. Materials

OREVAC[®] CA 100 from Arkema was considered as PPgMA. Ionic liquids supplied from TCI (Scheme 1) were selected according to the nature of the cation (combined with the same anion), i.e., tributyl (ethyl) phosphonium diethyl phosphate (P⁺DEP) vs. 1-ethyl-3-methylimidazolium diethyl phosphate (EMIM DEP). The nature of the anion was also considered by comparing the same cation, i.e., 1-ethyl-3-methylimidazolium acetate (EMIM Ac) vs. 1-ethyl-3-methylimidazolium diethyl phosphate (EMIM DEP).



Scheme 1. Structure of the ionic liquids considered in this study.

2.2. Material Preparation and Characterizations

The PPgMA was dried at 70 °C for 12 h. The PPgMA/IL mixtures (2 and 10 wt%) were blended into a DSM micro extruder at 180 °C for 5 min and injected at 30 °C. Three different Llonomer types, i.e., depending on the nature of the (cation/anion) pair and of IL content were prepared (Table 1).

Table 1. PPgMA/IL blends considered in this study.

Polymer	IL	IL Content (wt%)	Abbreviation
PPgMA	P ⁺ DEP	2	L-P ⁺ DEP-2
	P ⁺ DEP	10	L-P ⁺ DEP-10
	EMIM DEP	2	L-EMIM DEP-2
	EMIM DEP	10	L-EMIM DEP-10
	EMIM Ac	2	L-EMIM Ac-2
	EMIM Ac	10	L-EMIM Ac-10

The morphology of samples was carried out by transmission electron microscope (TEM, Phillips CM 120) at an accelerating voltage of 120 kV. To characterize PPgMA and Llonomer, they are cut using ultramicrotomy firstly and collected on a carbon film-coated cooper grid.

The chemical interactions between PPgMA and ILs were characterized by NMR spectroscopy. ¹H and ³¹P NMR spectra of ionic liquids and Llonomers processed on PPgMA8 (8 wt% MA) were recorded using a Bruker Avance III 400 MHz at 373 K. Thanks to the relatively good solubility as well as the chemical nature (without any interactions with samples) of chlorobenzene-D5 (C₆D₅Cl), it has been selected as the NMR solvent. The chemical shifts (δ) are expressed in ppm relative to the internal reference C₆D₅Cl for ¹H nuclei.

The rheological and dynamic mechanical analysis (DMA) were performed using a ARES-G2 rheometer (ARES-G2 SN#4010-0255, TA Instrument, New Castle, DE, USA). The rheological behavior was recorded at 180 °C using parallel plate geometry (d = 25 mm) under N₂ atmosphere. Dynamic mechanical curves were recorded in the −80/100 °C temperature range with a heating rate of 3 K·min^{−1}.

Melting and crystallization curves were recorded by Differential Scanning Calorimetry (DSC, Q10 TA Instrument, New Castle, DE, USA) after erasing the thermal history under 5, 10, and 20 K·min^{−1} heating and cooling rates. The crystallinity, X_c, was defined using Equation (1):

$$X_c = \frac{\Delta H_f}{(1 - m)\Delta H_f^0} \quad (1)$$

where ΔH_f^0 is 209 J/g, i.e., corresponding to the melting enthalpy of 100% crystallized polymer [27], ΔH_f being the melting enthalpy of the analyzed sample. Jeziorny's [28] non-isothermal crystallization model was employed to analyze the crystallization process:

$$\ln[-\ln(1 - X_t)] = n \ln t + \ln Z_t \quad (2)$$

$$X_T = \frac{\int_{T_0}^{T_c} \left(\frac{dH_c}{dT} \right) / dT}{\int_{T_0}^{T_\infty} \left(\frac{dH_c}{dT} \right) / dT} \quad (3)$$

$$t = \frac{T_0 - T}{\varphi} \quad (4)$$

where X_t is the relative crystallinity at crystallization time t ; n , and Z_t correspond to Avrami' exponent and crystallization kinetic constant, respectively. Their values can be obtained by plotting $\ln[-\ln(1 - X_t)]$ as a function of $\ln t$. X_T is related to the crystallinity with the change of temperature, T_0 and T_∞ being the onset and the end of crystallization temperature; T is the temperature for a given crystallization time t , while φ is the cooling rate.

The crystallization half-time ($t_{1/2}$) could be determined from Equation (5):

$$t_{1/2} = \left(\frac{\ln 2}{Z_t} \right)^{1/n} \quad (5)$$

The crystalline phase of the samples was analyzed by Wide Angle X-Ray Diffraction (WAXD, Bruker D8-Advance diffractometer) at room temperature ($2\theta = 10\text{--}45^\circ$ using Cu $K\alpha$ radiation – $\lambda = 0.15406$ nm). The diffractograms were further analyzed using Origin 2018 software considering Gauss' fitting function. The crystal size was calculated according to the Scherrer's equation:

$$D = \frac{K\lambda}{(\beta - s)\cos(\theta)} \quad (6)$$

where D is the crystal size, K the crystalline shape parameter (≈ 0.89), β the measured sample diffraction peak half-height width, s the instrument factor calibration (0.05°), and θ the diffraction angle.

The crystalline morphology of PPgMA and Llonomers materials was observed by polarizing optical microscopy (POM). Materials were heated at 200°C and remained for 3 min to eliminate the thermal history. Their crystal growth was observed after cooling at 120°C with a cooling rate of $50\text{ K}\cdot\text{min}^{-1}$.

The strain–stress curves were recorded using an Instron tensile machine at room temperature operating at a strain speed of $50\text{ mm}\cdot\text{min}^{-1}$. Each sample (dumbbell-shaped specimen with the geometry $T = 2\text{ mm}$, $w_0 = 12\text{ mm}$, $w = 4\text{ mm}$, $L = 30\text{ mm}$, $D = 45\text{ mm}$, $L_0 = 73.5\text{ mm}$) has been repeated at least three times. In order to avoid the influence of water, all the prepared samples are stored in a dry and cold environment and placed in the oven at 80°C for 4 h before test.

3. Results and Discussion

3.1. Llonomer Morphology

Transmission electron microscopy (TEM) is an efficient tool to study the phase separation of IL ion pairs within the polymer matrix (Figure 2). Owing to the expected morphologies of Llonomers, these granular "bean spots" could be attributed to phase-separated and associated ILs. IL-based aggregates can be also confirmed by EDX analyses as shown in Figure S1 of Supporting Information (spectra 1 in L-EMIM DEP-10: C: 85 wt%, N: 3 wt%, O: 11 wt%, P: 1 wt%; spectra 1 in polymer matrix in L-P⁺DEP-10: C: 97 wt%, O: 3 wt%; spectra 1 in L-P⁺DEP-10: C: 94 wt%, O: 5 wt%, P: 1 wt%; spectra 1 in L-EMIM Ac-10: C: 90 wt%, N: 2 wt%, O: 8 wt%). From comparison between L-P⁺DEP-10 (Figure 2c) and L-EMIM DEP-10 (Figure 2b), the previous one displays large ionic clusters, while the second one exhibits a multiscale structure based on not only large ionic liquid particles but

also ionic multiplets (black spots) due to associated cation-anion pairs. These multiplets and particles dual microstructure are more pronounced in L-EMIM Ac-10 (Figure 2d), and numerous multiplets are observed compared to L-EMIM DEP-10 (Figure 2b). These various types of sub-structures of prepared Llonomers are strongly dependent on the ion pair nature of the ILs. In fact, it is possible to predict theoretically the aggregation of ion pairs or multiplet structures in a low dielectric medium. Both are influenced by polar-polar interactions that are responsible for the differences in size. The resulting morphology of the ionic liquid interactions is related to the equilibrium of interactions between the grafted-PP matrix and ILs. In fact, the size of the IL-rich phase could be tailored from nanoscale to microscale by a proper selection of the cation/anion combinations [29].

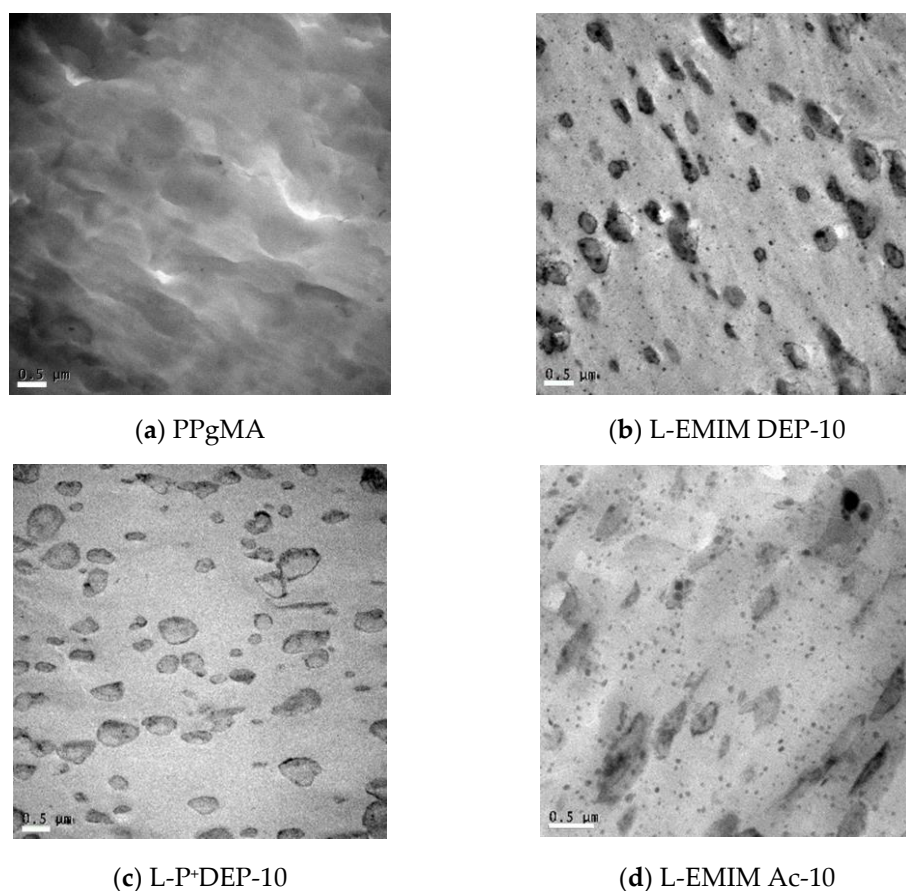


Figure 2. Transmission Electron Microscopy (TEM) images of PPgMA and related Llonomers containing 10 wt% of IL (scale bar: 0.5 μm), (a) PPgMA; (b) L-EMIM DEP-10; (c) L-P+DEP-10; (d) L-EMIM Ac-10.

3.2. PPgMA–ILs Interactions

^1H and ^{31}P NMR spectroscopy were recorded to detect IL-polymer chain interactions from the comparison between neat IL spectra and the ones from corresponding Llonomer as shown in Figures 3 and 4, respectively. In the case of EMIM Ac and the corresponding Llonomers, ^1H NMR spectra reveal a shift of the protons on the cation (positions #6, #2, and #3 of EMIM Ac), from 10.85, 8.49, and 8.64 ppm [30,31] to higher fields, i.e., 10.09, 8.09, and 8.01 ppm. Such shifts could be attributed to the enhancement of electronic cloud density (e-cloud density) because of the ionic-ionic interactions between the cation and polymer matrix (Figure 5a). Thus, the COO^- group, i.e., the counter anion of the IL is positioned near the maleic anhydride group, then the counter anion participates in the opening of maleic anhydride leading to the formation of a new structure “ionic-branched chains” via the electrostatic interaction among cation/anion in EMIM Ac. In addition, the hydrogens in positions #2 and #3 of terminal cation may be positively shielded by $\text{C}=\text{O}$ in the matrix. Besides, the hydrogen moving from 1.94 into 2.07 ppm at position #7 confirms the capture

of the hydrogen carried by the imidazolium cation, thus inducing the generation of acetic anhydride group.

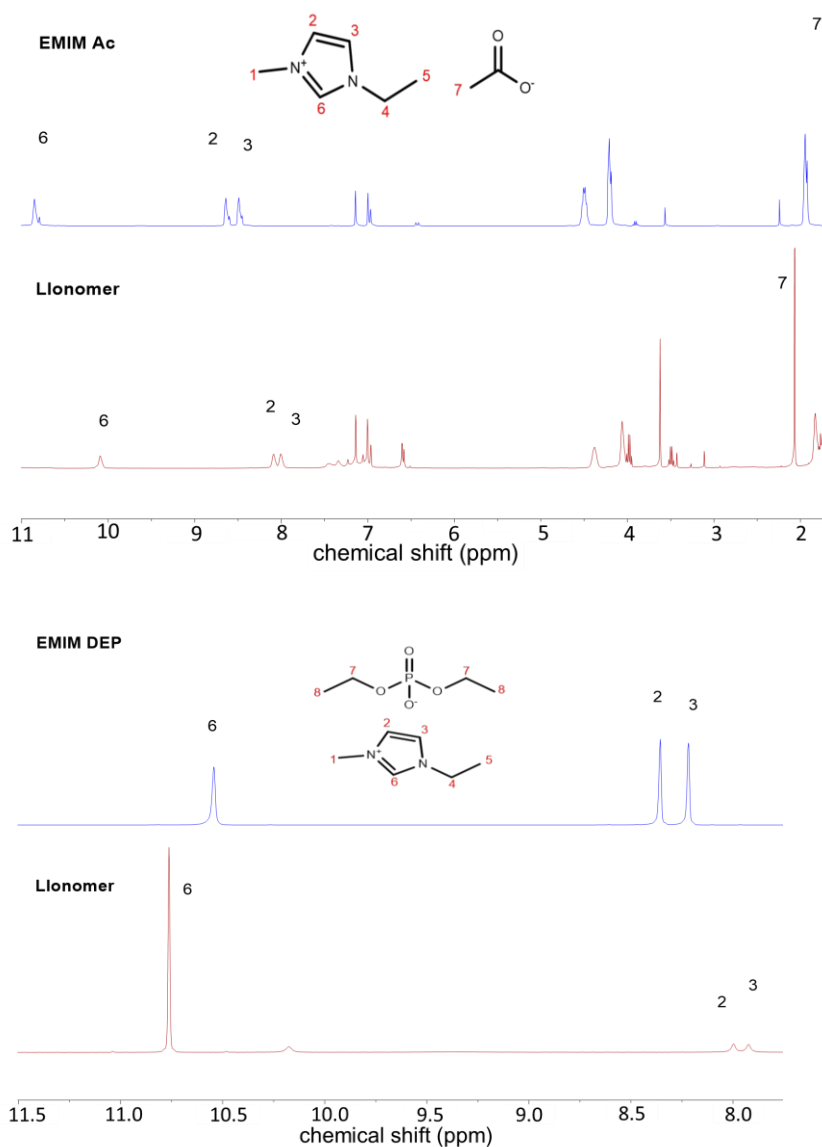


Figure 3. ¹H NMR spectra (400 MHz; C₆D₅Cl solvent) of ILs and related Llonomers materials (10 wt.% IL).

In addition to the enhanced e-cloud density at positions #2 and #3 (from 8.22 and 8.36 ppm of neat EMIM DEP [32,33] into 7.25 and 7.30 ppm of its Llonomer) as a result of the positive shielding effect of C=O in matrix (Figure 5b), the e-cloud density at position #6 decreases due to the strong electronic absorption capacity of oxygen in COO[−] in matrix, thus its hydrogen shifts from 10.54 to 10.76 ppm. In fact, the same phenomenon is also observed with imidazolium IL combined with acetate or phosphate counter anions. In terms of the phosphonium IL combined with phosphate counter anion, the phosphorous compound of the anion displays a movement into low field (from 0.18 in EMIM DEP to 0.57 ppm in Llonomer) because of the effect of connected C=O group in matrix. In addition, the e-cloud density of phosphorus in P⁺DEP anion increases (³¹P NMR from −0.38 ppm into −0.95 ppm) since it lies in the positive shielded area induced by connected C=O (Figure 5c), while the strong electronegativity of oxygen in generated COO[−] of matrix results in the migration in ³¹P NMR from 34.64 ppm into 34.99 ppm.

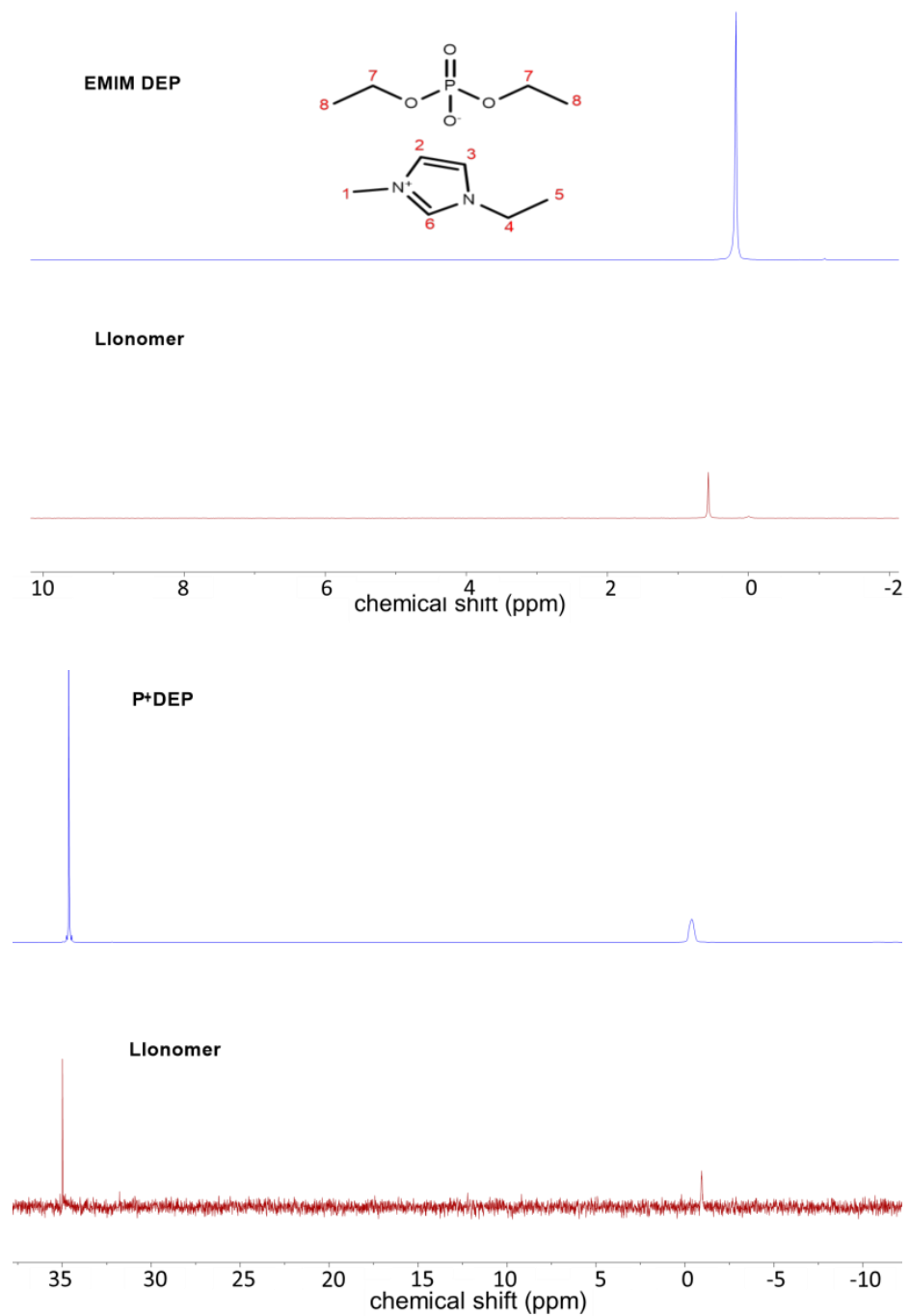


Figure 4. ^{31}P NMR spectra (400 MHz; $\text{C}_6\text{D}_5\text{Cl}$ solvent) of neat ILs and Llonomers (10 wt.% IL).

In summary, one may obtain that *a* all introduced ILs (EMIM Ac, EMIM DEP and P⁺DEP) can interact ionically with polar units in matrix; *b* the interaction structures between ILs and matrix varies with the change of anion/cation combinations; *c* the exceed ILs arrange as one ionic-branched chains using the generated COO^- group in PPgMA as the “head” and the cation/anion as the component via their original electrostatic interaction, such different interactions may connect the various dispersion of ILs in PPgMA and bring about some improvements into the overall performance (like molten viscosity, crystallization behavior, and so on).

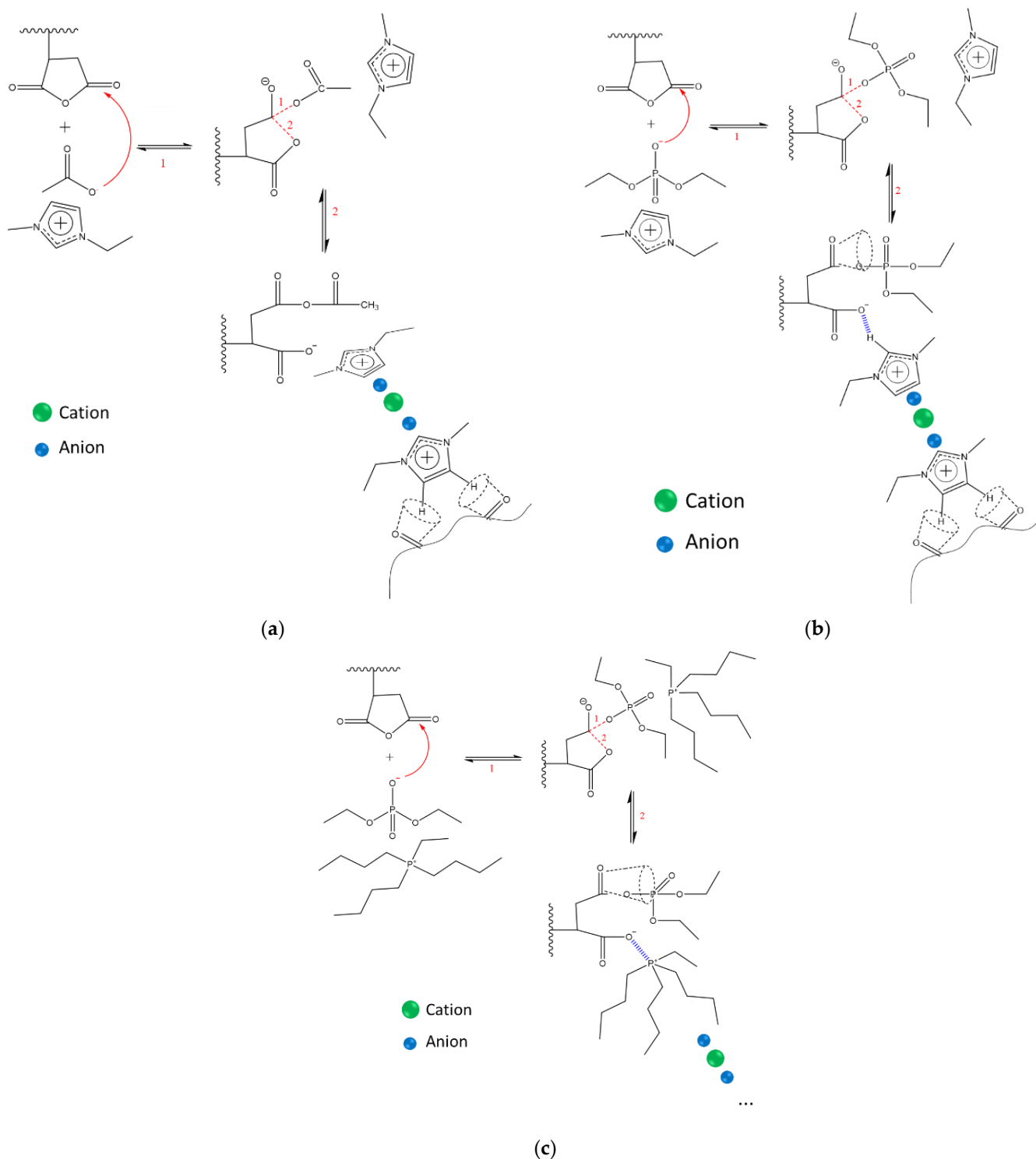


Figure 5. The various types of interactions which could be established between ionic liquid pairs and PPgMA within the different Llonomers materials considered in this study (based on: EMIM Ac: (a); EMIM DEP: (b); P⁺DEP: (c).

3.3. Effect of ILs on Rheological Properties: Strength of Interactions

The molten state behavior of Llonomers has been greatly changed compared to the neat PPgMA one due to the existence of the ion–ion/ion–dipolar interactions described previously. All Llonomers display a strong shear thinning behavior compared to neat PPgMA as shown in Figure 6. This effect is more pronounced for L-EMMI Ac-10. Owing to

the low viscosity of ILs (few mPa·s) [21], only the COO^- /IL combined with IL/IL interactions could induce inter-chains connecting nanostructures as reported in ionomers [3]. Such ionic branching nanophases lead to a reduction of the chain mobility, resulting in a large increase of the melt viscosity [8,16,34–36]. For each Llonomers, the complex η^* value increases with the ILs content, as more ionic interchain connections are formed. Such viscosity values dependence with the nature of the ionic liquid and its content could be easily explained according to the previously reported interactions. In fact, the viscosity value of Llonomer processed with EMIM Ac is the highest one because the ionic interactions between imidazolium cation and carboxylic acid is the strongest one (three positions could create ionic–ionic interactions with carboxylic group as shown in Figure 5a). Additionally, the acetate anion is also highly polar and could be strongly associated with cation. These cation-anion pairs could also self-assemble to form multiplets and lead to this double scale structuration observed by TEM. For the Llonomer with 10 wt% EMIM DEP, a double structuration is observed with not only ionic liquid-rich particles but also ionic multiplets. Compared with Llonomers prepared with EMIM Ac, less fine phase separation is obtained due to ionic–ionic (1 position) and dipolar–ionic (2 positions) interactions (Figure 5b) generated to a lesser extent. The numerous multiplets act as branching agents, leading to increase the viscosity. The morphology as well as the strength of the interaction explain the ranking of viscosity values. Thus, clusters-based morphology, i.e., without larger multiplet structures, combined with the low intensity interactions established between the phosphonium cation and the carboxylate anion explain the lowest viscosity of Llonomers prepared with the phosphonium cation. Besides, the sequence of corresponding solid density, i.e., $0.909 \text{ g}\cdot\text{cm}^{-3}$ of PPgMA $< 0.910 \text{ g}\cdot\text{cm}^{-3}$ of L-P⁺DEP-10 $< 0.915 \text{ g}\cdot\text{cm}^{-3}$ of L-EMIM DEP-10 $< 0.917 \text{ g}\cdot\text{cm}^{-3}$ of L-EMIM Ac-10 at around 20 °C could reveal the generation of ionic network within Llonomers, which could also reflect the interaction strength and is consistent with the resulted ranking of viscosity values.

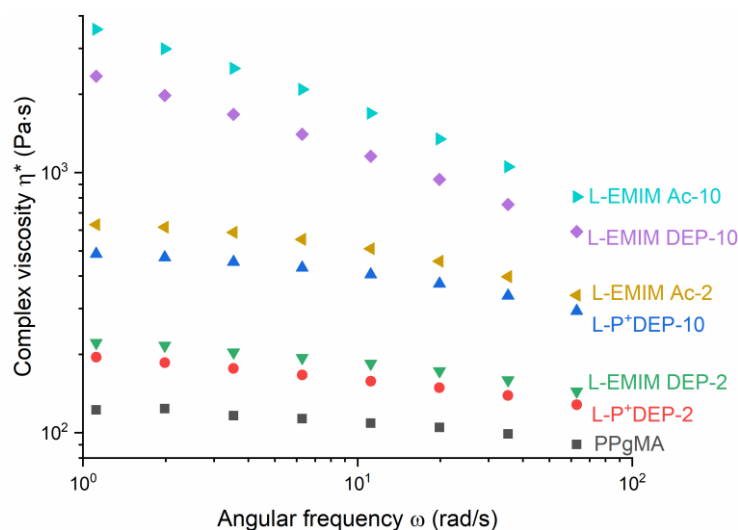


Figure 6. Complex viscosity of neat PPgMA and Llonomers as a function of the dynamic angular frequency at 180 °C.

3.4. Microstructure of Llonomers

Semi-crystalline polymers are considered to be a heterogeneous medium including crystalline fraction (CF), rigid amorphous fraction (RAF), and mobile amorphous fraction (MAF) [37]. Ordered crystalline chains constitute the CF phase, which is surrounded by macromolecular chains in the amorphous state [37,38]. Close to the CF lamellas, the neighboring polymer chains in amorphous state—denoted as tie molecules—undergo strong confinement effects and the reduction of segmental motions. As a consequence, this reduced molecular mobility of this confined amorphous phase may result in its own glass transition

temperature, different from the glass transition of chains in MAF. The amorphous fraction close to the crystalline fraction is denoted as RAF. Identifying the location of ILs in the final Llonomers materials could help understanding the structuration mechanisms and their effect on the overall performance of Llonomers. The solid state Dynamic Mechanical Analyses reveal two relaxations of the amorphous, i.e., the ones of the MAF and RAF regions. Figure 7 and Table 2 indicate the temperature of the α and α' relaxations related of the MAF and RAF fractions respectively, as well as the one of the β secondary relaxation (at -47 °C) of PPgMA. Such a relaxation corresponds to T_β local segmental motions [39]. As various types of IL are combined with PPgMA, the temperature of this β relaxation supports the idea that ionic interactions don't affect the local segmental motions of PPgMA. Similarly, T_α (MAF) of Llonomers associated to the glassy transition temperature remain the same as neat PPgMA one.

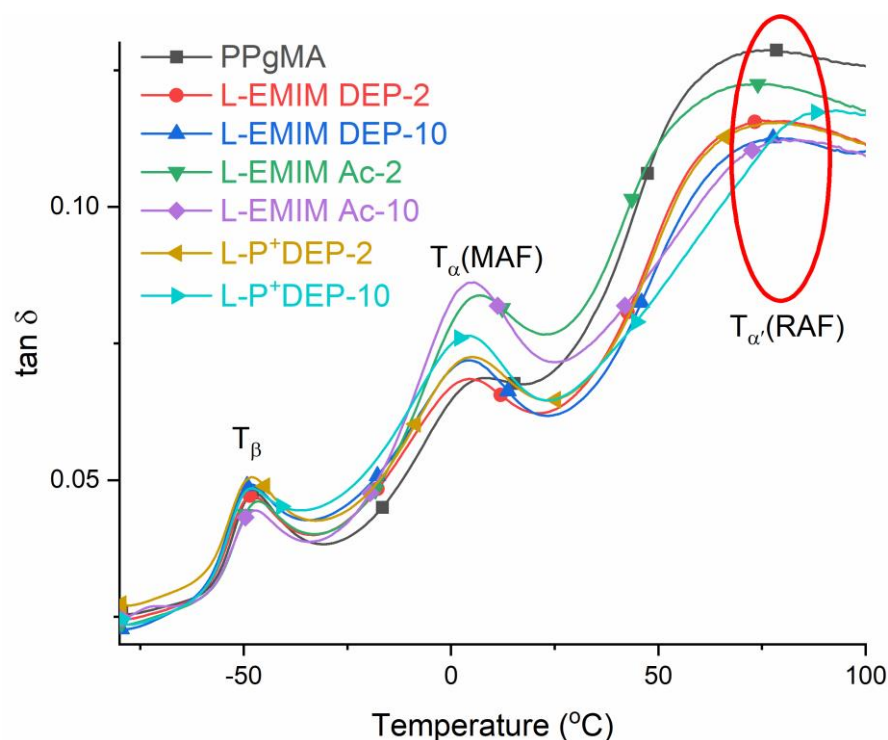


Figure 7. Loss factor ($\tan \delta$) vs. temperature for Llonomers at 1 Hz.

Table 2. Temperatures at the maximum of $\tan \delta$ at 1 Hz of the β , α and α' relaxations of neat PPgMA and associated Llonomers.

Materials	T_β (°C)	T_α (MAF, °C)	$T_{\alpha'}$ (RAF, °C)
PPgMA	-47	7	76
L-P ⁺ DEP-2	-47	5	79
L-P ⁺ DEP-10	-47	5	93
L-EMIM DEP-2	-47	5	74
L-EMIM DEP-10	-48	5	78
L-EMIM Ac-2	-47	7	78
L-EMIM Ac-10	-47	6	80

But the effect of P⁺DEP on the α' relaxation (RAF) is more pronounced (93 °C of Llonomer L-P⁺DEP-10), which involves the mobility of the confined chains close to the crystalline lamellae [22,40,41]. The same trend could be also observed from L-P⁺DEP-2 but to a lesser extent since the ionic liquid content is lower. This effect may be attributed to the preferential localization of these ILs in the RAF phase. The chemical structure of ILs could explain their influence on the relaxation spectra of Llonomers. The strong interactions

between ionic liquids and polar group within EMIM Acetate-based Llonomers highlighted by NMR and rheology account for the corresponding higher $T_{\alpha'}$ value than that of EMIM DEP-based Llonomers. While for L-P⁺DEP-10, the alkyl chains of the phosphonium cation could promote the miscibility with PPgMA.

3.5. Effect of ILs on Crystallization of PPgMA

3.5.1. Role of ILs in the Crystallization Process

Some works have already reported the influence of ILs on crystallization of semi-crystalline thermoplastics. For example, it was shown that phosphonium-based ILs could reduce the crystallinity (X_c) and crystallization temperature (T_c) of P(VDF-CTFE) [22,40]. In this work dedicated to maleic anhydride polypropylene/IL blends, no significant change of X_c could be observed (see Table 3 from Figure S2 and Table S1). This phenomenon is related to the location and distribution of ILs within Llonomers. It agrees with the previous conclusions on the fact that PPgMA and ionic liquids exist as separated phases. The ion–ion and ion–dipole interactions occur at the interface between phases. On the other hand, the temperature of crystallization of PPgMA, T_c , increases with the addition of a small amount of P⁺DEP or EMIM DEP, i.e., ILs having a phosphate anion, and retrieve almost the value of neat PPgMA with 10 wt.% of IL. The addition of EMIM Ac has no influence on T_c whatever its content.

Table 3. The T_c , $t_{1/2}$, and X_c values measured by DSC (heating and cooling rates: 5 K·min^{−1}).

Materials	X_c (%)	T_c , (°C)	$t_{1/2}$ (min)
PPgMA	34.1	116.1	0.77
L-P ⁺ DEP-2	37.6	126.8	0.74
L-P ⁺ DEP-10	35.1	116.0	0.76
L-EMIM DEP-2	36.8	124.6	0.72
L-EMIM DEP-10	35.3	118.0	0.86
L-EMIM Ac-2	34.2	118.8	0.77
L-EMIM Ac-10	36.9	118.5	0.72

DSC analyses of non-isothermal crystallization kinetics as well as observations by polarized optical microscopy (POM) can be used to detect the overall or partial crystallization process of PPgMA and Llonomers. The $\ln[-\ln(1 - X_t)]$ vs. $\ln t$ plots according to Jeziorny's non-isothermal crystallization model are shown in Figure S3 and Table S1. The value of $t_{1/2}$ (half-time crystallization) represents the time consumed to half crystallize, i.e., a longer time indicates a slower crystallization rate. As mentioned previously for the other parameters, $t_{1/2}$ slightly depends on (i) the nature of ion–ion and dipole–ion interactions within Llonomers that could delay the process of regular chain folding to generate the crystalline fraction, since the chain motions to change the configuration are restricted by nearby ILs involved in the interactions [22,40] ($t_{1/2}$: 0.86 min of L-EMIM DEP-10 vs. 0.77 min of PPgMA); (ii) the IL content, since high IL content may induce more interactions, followed by a greater impact on the crystallization process ($t_{1/2}$: 0.74 min of L-P⁺DEP-2 vs. 0.76 min of L-P⁺DEP-10; 0.72 min of L-EMIM DEP-2 vs. 0.86 min of L-EMIM DEP-10); (iii) the intensity of interactions could inhibit the movement of chain segment with some different extent, i.e., the restriction of chain motion caused by ion–ion interactions is stronger than that due to dipole–ion interactions. As a consequence, it results in a slower crystallization rate (L-EMIM DEP-10 vs. L-P⁺DEP-10); (iv) the miscibility of DEP anion in PPgMA promotes the crystallization process at low content.

In addition to the impact of the existing interactions within Llonomers on the crystallization process, IL itself may also influence the nucleation process. From the comparison of pure PPgMA matrix and Llonomers processed with 10 wt.% IL (at 5 K·min^{−1}, Table 3), L-EMIM Ac-10 crystallizes faster than all other systems. Because EMIM Ac could restrict the generation of nuclei (as shown in POM images a vs. d, a' vs. d' Figure 8) and cause a larger volume for the growth of the generated spherulites.

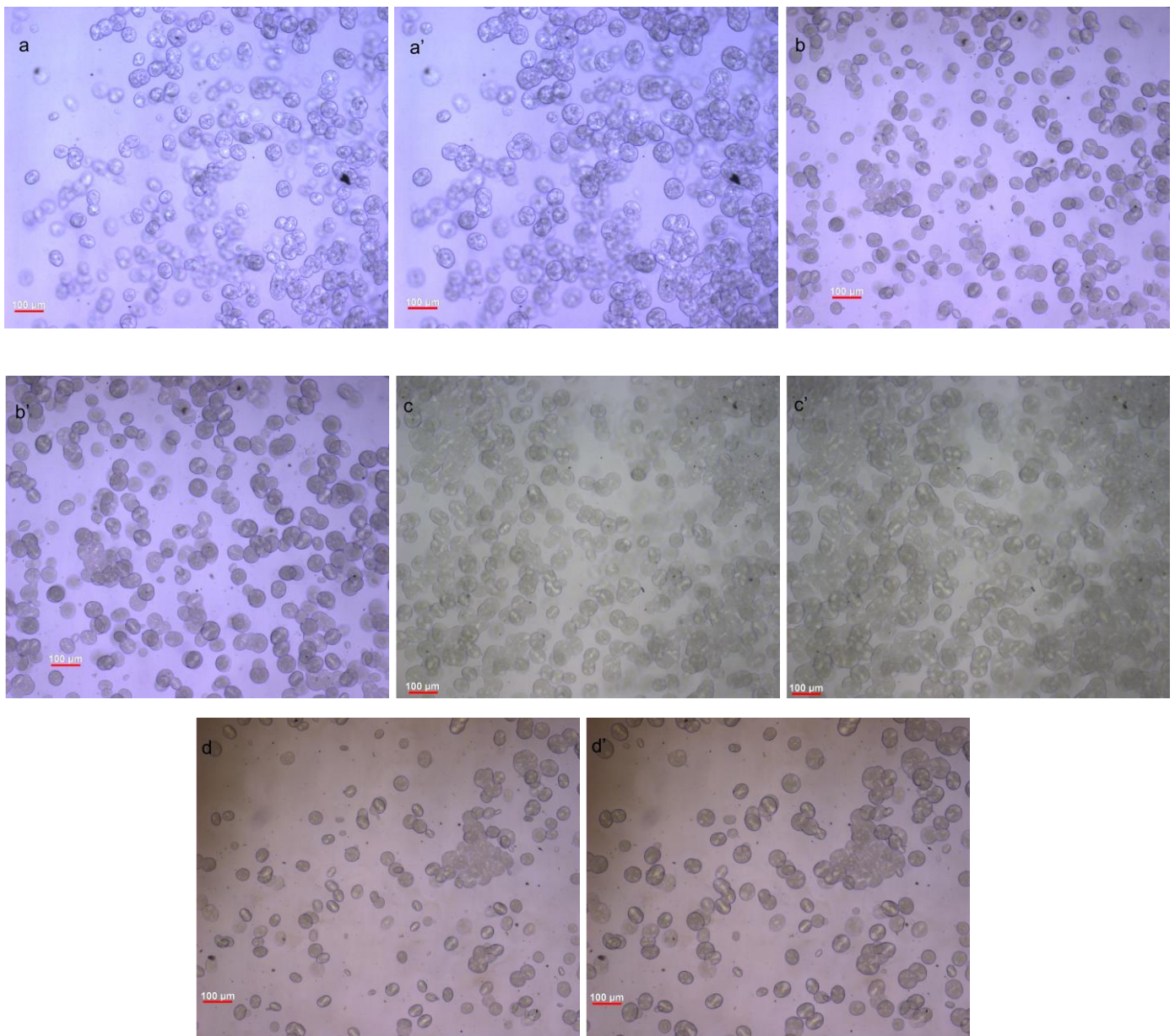


Figure 8. POM microscopies of PPgMA and Llonomers as a function of annealing time at 120 °C (scale bar 100μm): PPgMA (a) 80 s, (a') 100 s; L-P⁺DEP-10 (b) 80 s, (b') 100 s; L-EMIM DEP-10 (c) 70 s, (c') 90 s; L-EMIM Ac-10 (d) 100 s, (d') 120 s.

3.5.2. Effect on Crystalline Phase

As shown in Figure 9, the PPgMA crystallizes according to the syndiotactic monoclinic system, mainly in α type crystalline form characterized by the Bragg diffraction peaks at $2\theta \approx 14.0^\circ$ [110], 16.8° [040], 18.4° [130], 25.3° [060&150], 28.5° [220], and 42.6° [212]. A very weak diffraction peak belonging to (002) plane of the syndiotactic monoclinic [42] can also be detected at 23.6° . γ -form diffraction peak is not observed in the XRD profile (21.4° [α 111& γ 202]) because it is very difficult to distinguish γ -form from α -form diffraction peaks. γ -form cannot be present in this case, as the generation of this form requires specific crystallization conditions such as high pressure [43]. In Llonomers, most of diffraction peaks of PPgMA are not modified, but a new peak at $2\theta \approx 16.0^\circ$ belonging to β (300) could

be observed when 10 wt.% of EMIM DEP and EMIM Ac ILs are considered. The relative content of β -phase can be calculated from the Equation (7):

$$K = \frac{I_{300}}{I_{300} + I_{110} + I_{040} + I_{130}} \quad (7)$$

where I_{300} , I_{110} , I_{040} , and I_{130} are the intensities of the corresponding monoclinic phase diffraction reflections at $2\theta \approx 16.0$, 14.0 , 16.8 , and 18.4 respectively [44].

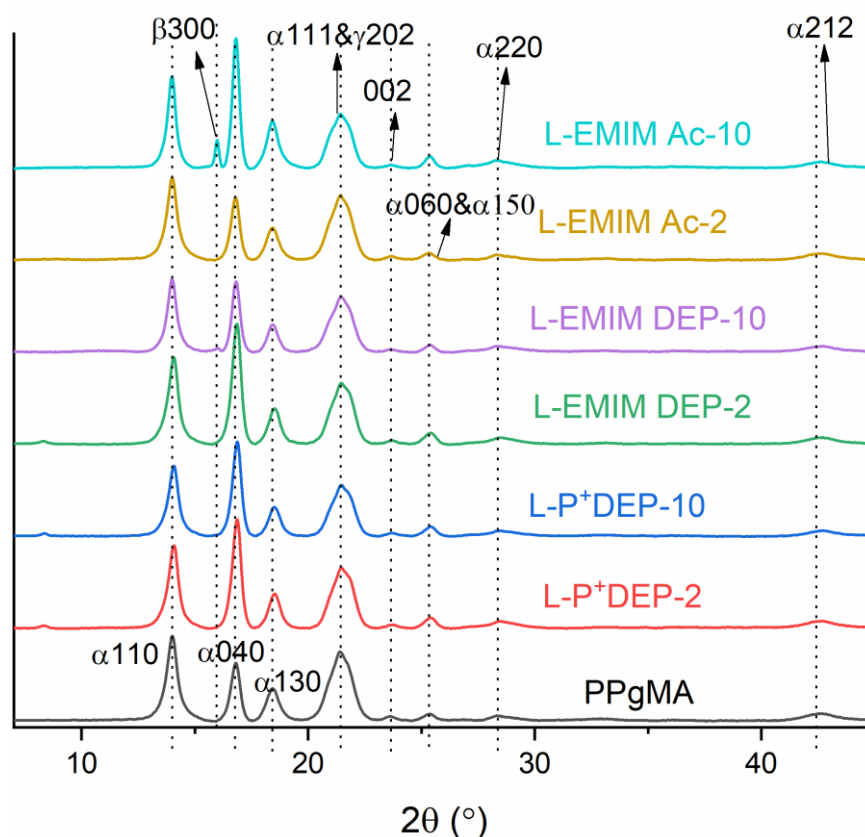


Figure 9. XRD diffraction patterns of PPgMA and its L-ionomers based on various ILs at different IL contents.

The generation of β -phase in L-ionomers based on EMIM DEP and EMIM Ac is related to the existence of stronger ion–ion and ion–dipole interactions with PPgMA than ones generated with P⁺DEP. These interactions within L-EMIM DEP-10 and L-EMIM Ac-10 restrain the folding and rearrangement of polymer chains into ordered conformation, resulting in the β -phase which is less stable crystalline form than the α -form. On the other side, L-ionomer based on 10 wt.% EMIM Ac exhibits larger β -form area than one obtained with the addition of 10 wt.% EMIM DEP (9.6% vs. 3.2%; see Table 4). As these two ILs hold the same cation (EMIM⁺), the extent-of-influence of these ILs on crystallinity morphology is associated with their interaction patterns (in NMR analysis) and the size of the anion (acetate vs. phosphate). More ion–ion positions contribute EMIM Ac to reinforce interactions, while the bigger and less interactive anion makes EMIM DEP less prone to promote strong interaction. The strongest ion–ion and ion–dipole interactions within L-ionomers can be correlated to their rheological behavior.

Table 4. XRD analyses of the PPgMA and its related Llonomers (from Figure 9).

	$D_{[110]}$ (nm)	$D_{[040]}$ (nm)	$D_{[130]}$ (nm)	$D_{[300]}$ (nm)	K (%)	Average Size (Å) ^a
PPgMA	12.7	18.2	12.8	-	-	12.7
L-P ⁺ DEP-2	13.5	18.2	14.1	-	-	12.3
L-P ⁺ DEP-10	13.6	18.3	13.8	-	-	12.4
L-EMIM DEP-2	13.3	18.0	13.7	-	-	12.5
L-EMIM DEP-10	8.9	21.0	15.8	72.4	3.2	13.1
L-EMIM Ac-2	13.0	18.6	13.0	-	-	12.6
L-EMIM Ac-10	17.4	24.3	13.0	51.2	9.6	14.0

where D is the crystallite size. ^a These values are calculated based on their α -crystalline form size.

3.6. Effect of ILs on Mechanical Behavior of Llonomers

Owing to the generated interactions and the structuration of the ILs within PPgMA matrix which can be tuned by the nature of ILs, i.e., the type of the anion and cation, the mechanical behavior of Llonomers can be also tailored. At low content of ILs, the Young's modulus significantly increases whatever the nature of the ionic liquid, as shown in Figure 10 and Table 5. With the addition of a large amount of ILs, the modulus decreases significantly due to the presence of large separated IL-rich phases that act as defects except for L-EMIM Ac-10. In the latter case, strong ion–dipole interactions have been confirmed and the specific mechanical behavior of this Llonomer agrees with rheology results. On the other side, the strain at break increases dramatically for Llonomers based on imidazolium cation unlike phosphonium cation. Based on the DSC and WAXD results, especially crystallinity rates and morphisms, the generation of β -phase caused by strong ion–ion/dipole–ion interactions and multiscale morphologies, i.e., ILs as clusters and separated phase, can explain the difference of strain at break observed from the various types of Llonomers. The addition of EMIM Ac (even at low content, i.e., 2 wt.%) leads to the enhancement of both Young's modulus and strain at break. The imidazolium cation plays a key role in the reinforcement of the mechanical properties. This cation leads to strong interactions with PPgMA that governs the macroscopic behavior of the corresponding Llonomers. The interactions based on phosphate anion are not sufficient to reinforce the mechanical behavior of the related Llonomers. The interactions are even stronger with the imidazolium cation and further when imidazolium is combined with acetate anion as more ion–ion interaction positions.

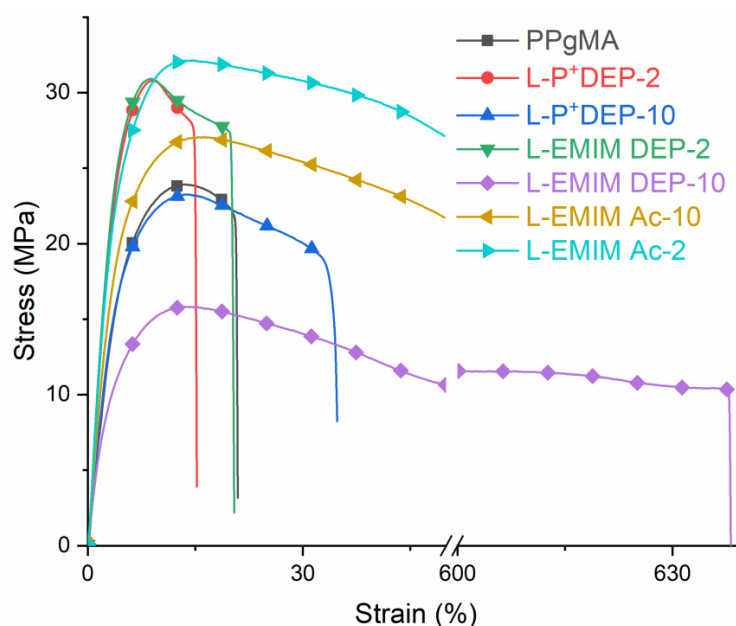
**Figure 10.** Stress–strain curves from tensile tests for of PPgMA and related Llonomers.

Table 5. Mechanical properties of PPgMA and related Llonomers (from tensile tests performed at room temperature).

Samples	Young's Modulus (MPa)	Strain at Break (%)	Yield Stress (MPa)
PPgMA	456 ± 18	24 ± 6	24 ± 1
L-P ⁺ DEP-2	705 ± 4	14 ± 3	30 ± 1
L-P ⁺ DEP-10	492 ± 12	35 ± 5	24 ± 1
L-EMIM DEP-2	803 ± 10	23 ± 2	31 ± 1
L-EMIM DEP-10	431 ± 11	655 ± 20	16 ± 1
L-EMIM Ac-2	756 ± 9	65 ± 4	31 ± 3
L-EMIM Ac-10	609 ± 12	550 ± 34	28 ± 1

In summary, it is worth noting that the introduced ionic liquids in grafted polypropylene don't behave as plasticizers, i.e., leading to decrease the Young's modulus and increase the strain at break as reported in the literature [22,40]. The mechanical behavior can be tailored to the nature of the cation and anion of the ionic liquid. For Llonomers, the slightly enhanced crystallinity rate contributes partly to the increase of stiffness while the multiscale distribution of ILs within the PPgMA matrix, i.e., as ionic multiplets and IL-separated phase, as well as strong ion–ion/dipole–ion interactions are the major contributors to the mechanical property of Llonomers.

4. Conclusions

From the combination of the maleic anhydride-grafted polypropylene (PPgMA) and three different ionic liquids, tributyl (ethyl)phosphonium diethyl phosphate (named P⁺DEP), 1-ethyl-3-methylimidazolium diethyl phosphate (named EMIM DEP), and 1-ethyl-3-methylimidazolium acetate (named EMIM Ac), Llonomers, i.e., a new generation of ionomers, have been successfully synthesized. This work reveals that the presence of grafted maleic anhydride on the polypropylene backbone as the “head group” combined with ionic liquid pairs could lead to the formation of new nanostructures via the generation of ionic and polar interactions. Different morphologies can be designed, i.e., from a phase separation resulting in a single-(nano) scale structuration composed of distribution of ionic clusters when Llonomers regarding phosphonium-based ILs, to a multi-scale structure combining ionic clusters but also IL-rich separated phase as for imidazolium cation-based ILs. The smaller size of the separated IL-rich phases is prone to establish the stronger ILs/polymer interactions. The imidazolium cation combined with the acetate anion appears as the most relevant IL to optimize the interactions with maleic anhydride group grafted onto the polypropylene backbone. The physical properties both in the molten and solid states appear to be strongly influenced by these interactions. In fact, the increase of the complex viscosity highlights the existence of IL/polymer interactions and the ability in such a case to form an ionic network. In relation with their morphology, crystallinity, and the existence of percolated ionic phase, Llonomers display both improved Young's modulus and ability to sustain large strains before break. Therefore, these Llonomers are very promising for processing functional materials such as foams or melt blown membranes.

Supplementary Materials: The following are available online at <https://www.mdpi.com/article/10.3390/polym15020370/s1>, Figure S1: Elemental analysis spectra (EDX) of Llonomers performed on fractured surfaces observed by TEM. Figure S2. DSC traces of PPgMA and related Llonomers prepared with various ionic liquids (2 and 10 wt.%). Melting and crystallization phenomenon was observed for different heating and cooling rates (5, 10, and 20 K·min⁻¹) under nitrogen atmosphere. Figure S3. $\ln[-\ln(1 - X_t)]$ vs. $\ln t$ plots according to Jeziorny's crystallization model for neat PPgMA and related Llonomers based on various ionic liquids (2 and 10 wt.%) for different cooling rates (5, 10, and 20 K·min⁻¹). Table S1. Parameters of non-isothermal crystallization process based on Jeziorny's model.

Author Contributions: L.H. did the experiments and analyzed the results as well as wrote this manuscript under the supervision of S.L., J.-F.G., and J.D.-R. All authors have read and agreed to the published version of the manuscript.

Funding: This research was funded by the CSC China Scholarship Council, grant number 201808510284 and the French Ministry of Higher Education, Research, and Innovation (MESRI).

Institutional Review Board Statement: Not applicable.

Informed Consent Statement: Not applicable.

Data Availability Statement: Not applicable.

Acknowledgments: Thanks for the financial support from the program of China Scholarship Council (No.201808510284). The authors would like to thank Pierre Alcouffe for the transmission electron microscopy, Ruben Vera for XRD measurements (Centre Henri Longchambon) experiments, Carlos Fernandez de Alba and Patrick Goetinck for NMR tests, while Celso Yassuo Okada Junior for NMR analysis.

Conflicts of Interest: The authors declare no conflict of interest.

References

1. Zhang, L.; Brostowitz, N.R.; Cavicchi, K.A.; Weiss, R.A. Perspective: Ionomer research and applications. *Macromol. React. Eng.* **2014**, *8*, 81–99. [[CrossRef](#)]
2. Kirkmeyer, B.P.; Weiss, R.A.; Winey, K.I. Spherical and vesicular ionic aggregates in Zn-neutralized sulfonated polystyrene ionomers. *J. Polym. Sci. Part B Polym. Phys.* **2001**, *39*, 477–483. [[CrossRef](#)]
3. Eisenberg, A.; Hird, B.; Moore, R.B. A new multiplet-cluster model for the morphology of random ionomers. *Macromolecules* **1990**, *23*, 4098–4107. [[CrossRef](#)]
4. Datta, S.; De, P.; De, S. Blends of ionomers. *J. Appl. Polym. Sci.* **1996**, *61*, 1839–1846. [[CrossRef](#)]
5. Longworth, R.; Vaughan, D.J. Physical structure of ionomers. *Nature* **1968**, *218*, 85–87. [[CrossRef](#)]
6. Kim, J.-S.; Yoshikawa, K.; Eisenberg, A. Molecular Weight Dependence of the Viscoelastic Properties of Polystyrene-Based Ionomers. *Macromolecules* **1994**, *27*, 6347–6357. [[CrossRef](#)]
7. Dalmas, F.; Leroy, E. New Insights into Ionic Aggregate Morphology in Zn-Neutralized Sulfonated Polystyrene Ionomers by Transmission Electron Tomography. *Macromolecules* **2011**, *44*, 8093–8099. [[CrossRef](#)]
8. Aitken, B.S.; Buitrago, C.F.; Heffley, J.D.; Lee, M.; Gibson, H.W.; Winey, K.I.; Wagener, K.B. Precision ionomers: Synthesis and thermal/mechanical characterization. *Macromolecules* **2012**, *45*, 681–687. [[CrossRef](#)]
9. Weiss, R.A.; Zhao, H. Rheological behavior of oligomeric ionomers. *J. Rheol.* **2009**, *53*, 191–213. [[CrossRef](#)]
10. Qiao, X.; Weiss, R.A. Nonlinear Rheology of Lightly Sulfonated Polystyrene Ionomers. *Macromolecules* **2013**, *46*, 2417–2424. [[CrossRef](#)]
11. Ling, G.H.; Wang, Y.; Weiss, R. Linear viscoelastic and uniaxial extensional rheology of alkali metal neutralized sulfonated oli-gostyrene ionomer melts. *Macromolecules* **2012**, *45*, 481–490. [[CrossRef](#)]
12. Rapone, I.; Taresco, V.; Lisio, V.D.; Piozzi, A.; Francolini, I. Silver-and Zinc-Decorated Polyurethane Ionomers with Tunable Hard/Soft Phase Segregation. *Int. J. Mol. Sci.* **2021**, *22*, 6134. [[CrossRef](#)]
13. Ro, A.J.; Huang, S.J.; Weiss, R. Synthesis and properties of random poly (lactic acid)-based ionomers. *Polymer* **2009**, *50*, 1134–1143. [[CrossRef](#)]
14. Ro, A.J. Synthesis and Properties of Poly(lactic Acid) Ionomers. Ph.D. Thesis, University of Connecticut, Mansfield, CT, USA, 2008.
15. Wu, M.-H.; Wang, C.-C.; Chen, C.-Y. Preparation of high melt strength polypropylene by addition of an ionically modified poly-propylene. *Polymer* **2020**, *202*, 122743. [[CrossRef](#)]
16. Li, Y.; Yao, Z.; Chen, Z.-H.; Qiu, S.-L.; Zeng, C.; Cao, K. High melt strength polypropylene by ionic modification: Preparation, rheological properties and foaming behaviors. *Polymer* **2015**, *70*, 207–214. [[CrossRef](#)]
17. Colbeaux, A.; Fenouillot, F.; Gérard, J.-F.; Taha, M.; Wautier, H. Compatibilization of a polyolefin blend through covalent and ionic coupling of grafted polypropylene and polyethylene. II. Morphology. *J. Appl. Polym. Sci.* **2004**, *93*, 2237–2244. [[CrossRef](#)]
18. Colbeaux, A.; Fenouillot, F.; Gérard, J.-F.; Taha, M.; Wautier, H. Compatibilization of a polyolefin blend through covalent and ionic coupling of grafted polypropylene and polyethylene. I. Rheological, thermal, and mechanical properties. *J. Appl. Polym. Sci.* **2005**, *95*, 312–320. [[CrossRef](#)]
19. Livi, S.; Duchet-Rumeau, J.; Pham, T.-N.; Gérard, J.-F. A comparative study on different ionic liquids used as surfactants: Effect on thermal and mechanical properties of high-density polyethylene nanocomposites. *J. Colloid Interface Sci.* **2010**, *349*, 424–433. [[CrossRef](#)]
20. Rahman, M.; Brazel, C.S. Ionic liquids: New generation stable plasticizers for poly (vinyl chloride). *Polym. Degrad. Stab.* **2006**, *91*, 3371–3382. [[CrossRef](#)]
21. Yousfi, M.; Livi, S.; Duchet-Rumeau, J. Ionic liquids: A new way for the compatibilization of thermoplastic blends. *Chem. Eng. J.* **2014**, *255*, 513–524. [[CrossRef](#)]
22. Yang, J.; Pruvost, S.; Livi, S.; Duchet-Rumeau, J. Understanding of versatile and tunable nanostructuring of ionic liquids on fluorinated copolymer. *Macromolecules* **2015**, *48*, 4581–4590. [[CrossRef](#)]

23. Leroy, E.; Jacquet, P.; Coativy, G.; Reguerre, A.L.; Lourdin, D. Compatibilization of starch–zein melt processed blends by an ionic liquid used as plasticizer. *Carbohydr. Polym.* **2012**, *89*, 955–963. [[CrossRef](#)]
24. Chen, Y.; Zhang, Y.; Ke, F.; Zhou, J.; Wang, H.; Liang, D. Solubility of neutral and charged polymers in ionic liquids studied by laser light scattering. *Polymer* **2011**, *52*, 481–488. [[CrossRef](#)]
25. Hajipour, A.R.; Rafiee, F. Recent progress in ionic liquids and their applications in organic synthesis. *Org. Prep. Proced. Int.* **2015**, *47*, 249–308. [[CrossRef](#)]
26. Yue, C.; Fang, D.; Liu, L.; Yi, T.-F. Synthesis and application of task-specific ionic liquids used as catalysts and/or solvents in organic unit reactions. *J. Mol. Liq.* **2011**, *163*, 99–121. [[CrossRef](#)]
27. Clark, E.J.; Hoffman, J.D. Regime III crystallization in polypropylene. *Macromolecules* **1984**, *17*, 878–885. [[CrossRef](#)]
28. Jeziorny, A. Parameters characterizing the kinetics of the non-isothermal crystallization of poly (ethylene terephthalate) determined by DSC. *Polymer* **1978**, *19*, 1142–1144. [[CrossRef](#)]
29. Livi, S.; Duchet-Rumeau, J.; Gérard, J.-F. Nanostructuring of ionic liquids in fluorinated matrix: Influence on the mechanical properties. *Polymer* **2011**, *52*, 1523–1531. [[CrossRef](#)]
30. Dibble, D.C.; Li, C.; Sun, L.; George, A.; Cheng, A.; Çetinkol, Ö.P.; Benke, P.; Holmes, B.M.; Singh, S.; Simmons, B.A. A facile method for the recovery of ionic liquid and lignin from biomass pretreatment. *Green Chem.* **2011**, *13*, 3255–3264. [[CrossRef](#)]
31. Clough, M.T.; Geyer, K.; Hunt, P.A.; Mertes, J.; Welton, T. Thermal decomposition of carboxylate ionic liquids: Trends and mechanisms. *Phys. Chem. Chem. Phys.* **2013**, *15*, 20480–20495. [[CrossRef](#)] [[PubMed](#)]
32. Dubey, S.; Bharmoria, P.; Gehlot, P.S.; Agrawal, V.; Kumar, A.; Mishra, S. 1-Ethyl-3-methylimidazolium diethylphosphate based extraction of bioplastic “Poly-hydroxyalkanoates” from bacteria: Green and sustainable approach. *ACS Sustain. Chem. Eng.* **2018**, *6*, 766–773. [[CrossRef](#)]
33. Binks, F.C.; Cavalli, G.; Henningsen, M.; Howlin, B.J.; Hamerton, I. Examining the influence of anion nucleophilicity on the polymerisation initiation mechanism of phenyl glycidyl ether. *Polymers* **2019**, *11*, 657. [[CrossRef](#)] [[PubMed](#)]
34. Weiss, R.A.; Yu, W.-C. Viscoelastic Behavior of Very Lightly Sulfonated Polystyrene Ionomers. *Macromolecules* **2007**, *40*, 3640–3643. [[CrossRef](#)]
35. Page, K.A.; Park, J.K.; Moore, R.B.; Garcia Sakai, V. Direct analysis of the ion-hopping process associated with the α -relaxation in perfluorosulfonate ionomers using quasielastic neutron scattering. *Macromolecules* **2009**, *42*, 2729–2736. [[CrossRef](#)]
36. Castagna, A.M.; Wang, W.; Winey, K.I.; Runt, J. Influence of cation type on structure and dynamics in sulfonated polystyrene ionomers. *Macromolecules* **2011**, *44*, 5420–5426. [[CrossRef](#)]
37. Ma, Q.; Georgiev, G.; Cebe, P. Constraints in semicrystalline polymers: Using quasi-isothermal analysis to investigate the mechanisms of formation and loss of the rigid amorphous fraction. *Polymer* **2011**, *52*, 4562–4570. [[CrossRef](#)]
38. Arnoult, M.; Dargent, E.; Mano, J. Mobile amorphous phase fragility in semi-crystalline polymers: Comparison of PET and PLLA. *Polymer* **2007**, *48*, 1012–1019. [[CrossRef](#)]
39. Bajsić, E.G.; Šmit, I.; Leskovic, M. Blends of thermoplastic polyurethane and polypropylene. I. Mechanical and phase behavior. *J. Appl. Polym. Sci.* **2007**, *104*, 3980–3985. [[CrossRef](#)]
40. Xing, C.; Zhao, M.; Zhao, L.; You, J.; Cao, X.; Li, Y. Ionic liquid modified poly (vinylidene fluoride): Crystalline structures, miscibility, and physical properties. *Polym. Chem.* **2013**, *4*, 5726–5734. [[CrossRef](#)]
41. Mijovic, J.; Sy, J.-W.; Kwei, T. Reorientational dynamics of dipoles in poly (vinylidene fluoride)/poly (methyl methacrylate)(PVDF/PMMA) blends by dielectric spectroscopy. *Macromolecules* **1997**, *30*, 3042–3050. [[CrossRef](#)]
42. Clark, E.S. Unit cell information on some important polymers. In *Physical Properties of Polymers Handbook*; Springer: Berlin/Heidelberg, Germany, 2007; pp. 619–624.
43. Yang, G.; Li, X.; Chen, J.; Yang, J.; Huang, T.; Liu, X.; Wang, Y. Crystallization behavior of isotactic polypropylene induced by competition action of β nucleating agent and high pressure. *Colloid Polym. Sci.* **2012**, *290*, 531–540. [[CrossRef](#)]
44. Zipper, P.; Janosi, A.; Wrentschur, E. Scanning X-ray scattering of mouldings from semicrystalline polymers. *J. De Phys. IV* **1993**, *3*, C8-33–C8-36. [[CrossRef](#)]

Disclaimer/Publisher’s Note: The statements, opinions and data contained in all publications are solely those of the individual author(s) and contributor(s) and not of MDPI and/or the editor(s). MDPI and/or the editor(s) disclaim responsibility for any injury to people or property resulting from any ideas, methods, instructions or products referred to in the content.